Robust Twin Pairs of Weyl Fermions in Ferromagnetic Oxides

B. W. Xia,[1] Y. J. Jin,[1] J. Z. Zhao,[1] Z. J. Chen,[1,2] B. B. Zheng,[1] Y. J. Zhao,[2] R. Wang,[1,3,*] and H. Xu[1,†]
[1]Department of Physics & Institute for Quantum Science and Engineering, Southern University of Science and Technology, Shenzhen 518055, People's Republic of China
[2]Department of Physics, South China University of Technology, Guangzhou 510640, People's Republic of China
[3]Institute for Structure and Function & Department of physics, Chongqing University, Chongqing 400044, People's Republic of China

(Received 23 July 2018; published 7 February 2019)

The ferromagnetic Weyl semimetals with inversion symmetry usually possess odd pairs of Weyl fermions. Here, we present an inversion eigenvalue argument to dictate the existence of even pairs of ferromagnetic Weyl fermions. We show, by a combination of first-principles calculations and symmetry analyses, that this exotic topological feature can be verified in ferromagnetic oxides in different space groups. In particular, a realistic candidate, i.e., hollandite $RbCr_4O_8$ with a high Curie temperature (~295 K), hosts intriguing twin pairs of Weyl fermions, which are robustly stable against perturbations. Moreover, our effective model and symmetry analysis show that the twin pairs of Weyl fermions originate from a mirrored nodal ring pair. The nontrivial surface states and Fermi arcs of $RbCr_4O_8$ are clearly visible, further revealing the topological features. This work strengthens the understanding of the parity analysis in exploring ferromagnetic topological materials with unconventional fermionic excitations.

DOI: 10.1103/PhysRevLett.122.057205

Topological semimetals have attracted extensive interest in recent years due to their exotic quantum phenomena, including novel transport properties and topological surface states [1]. The interplay of symmetry with band topology plays a crucial role in electronic band structures of topological semimetals, resulting in the topologically protected zero-dimensional pointlike or one-dimensional linelike Fermi surfaces in momentum space. Under different constraints of symmetries in crystals, topological semimetals highlight several types of low-energy excitations around protected band-crossing points, such as Dirac fermions [2,3], Weyl fermions [4–8], nodal line fermions [9], triple fermions [10], and hourglass fermions [11] as well as even beyond [12]. Furthermore, the exhaustive analysis for symmetry arguments to identify topological phases have been performed recently [13,14]. These quasiparticles in electronic band structures exhibit abundant topological features. Of particular interest are Weyl semimetals (WSMs), in which the Weyl points (WPs) with definite chirality act as monopoles in momentum space.

So far, the majority of predicted WSMs are nonmagnetic, and nonmagnetic Weyl fermions have successively been observed in angle resolved photoemission spectroscopy (ARPES) measurements [15,16]. In comparison with nonmagnetic WSMs, magnetic and especially ferromagnetic (FM) WSMs with time reversal symmetry ($\mathcal{T}$) breaking play more essential roles in the field. On the one hand, the nontrivial band structures coexisting with a magnetization in FM WSMs possess promising spintronics-related applications. On the other hand, the interplay between magnetic group with different spin alignments and symmetry provides an ideal platform to investigate the symmetry-protected topological order.

However, magnetic topological WSMs are very limited. Up to now, only several magnetic ones have been proposed, such as $R_2Ir_2O_7$ [4], $HgCr_2Se_4$ [6], Mn_3X ($X = Ge$, Sn) [17], magnetic Heusler alloys [18], centrosymmetric tetragonal structures [19], and CrO_2 [20]. Unfortunately, neither the topological quasiparticles nor their accompanying nontrivial surface states in FM WSMs have been directly observed in experiments due to the lack of suitable candidates. Although the theoretical analysis based on magnetic group has provided valuable guidelines, the search for realistic FM WSMs is still a huge challenge. It is well known that the product of the inversion eigenvalues in centrosymmetric FM WSMs at the eight time-reversal invariant momenta (TRIM) points is usually equal to -1, which results in odd pairs of WPs in FM WSMs [21,22]. Here we raise a follow-up question: is there a WSM to host even pairs of WPs? More importantly, it is urgent to develop a systematic approach using the parity arguments to classify FM WSMs with their attracted features.

We first elucidate an inversion eigenvalue argument in FM materials with inversion ($\mathcal{I}$) symmetry. The spin degeneracy of electronic bands is removed by $\mathcal{T}$ breaking; i.e., $\mathcal{I}^2 = -1$. As shown in Fig. 1, considering a parallelepiped with eight TRIM points as its vertices, the topological features are characterized by two parallel surfaces, e.g., the planes of $k_3 = 0$ and $k_3 = \pi$. The two-dimensional

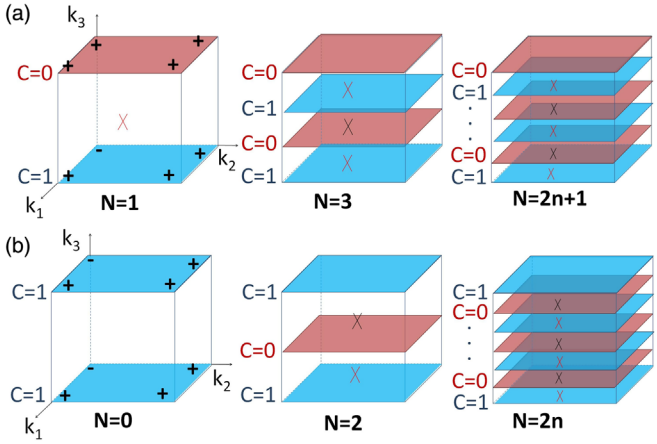

FIG. 1. Two distinct topological phases connect the parity analysis. (a) The product $\chi_p = -1$ with odd pairs of WPs. (b) The product $\chi_p = 1$ coexisting with $\mathcal{C}|_{k_3=0} = \mathcal{C}|_{k_3=\pi} = 1$, indicating that this system can be 3D Chern insulators (left panel) or WSMs with even pairs of Weyl points (middle and right panels). The representative parity eigenvalues at TRIM points are marked in the left panels of (a) and (b). The imaginary 2D cuts with the Chern numbers $\mathcal{C} = 1$ and $\mathcal{C} = 0$ are denoted by blue and maroon, respectively.

(2D) Hamiltonian $H(\mathbf{k})|_{k_3=0}$ and $H(\mathbf{k})|_{k_3=\pi}$ are both inversion symmetric. The individual Chern number for each plane can be expressed as [23]

$$\prod_{\mathbf{K}_{\rm inv}} \eta(\mathbf{K}_{\rm inv})|_{k_3=0,\pi} = (-1)^{\mathcal{C}[H(\mathbf{k})]|_{k_3=0,\pi}}, \tag{1}$$

where $\eta(\mathbf{K}_{\rm inv}) = \prod_n \eta_n(\mathbf{K}_{\rm inv})$, and $\eta_n(\mathbf{K}_{\rm inv})$ is the parity of occupied Bloch states at TRIM point $\mathbf{K}_{\rm inv}$. Equation (1) indicates that the Chern number connects the parity eigenvalues at TRIM points, which can be proved by an analysis of the Berry Phase in the Supplemental Material (SM) [23].

For a FM system with $\mathcal{I}$ symmetry, there are two distinct topological phases based on parity arguments as shown in Fig. 1. The one is that the product $\chi_p = \prod_{\mathbf{K}_{\rm inv}} \eta(\mathbf{K}_{\rm inv})$ at the eight TRIM points is -1. In this case, the two planes of $k_3 = 0$ and $k_3 = \pi$ possess the opposite Chern numbers, i.e., $\mathcal{C}|_{k_3=0} = 1$ and $\mathcal{C}|_{k_3=\pi} = 0$ [see Fig. 1(a)], and vice versa. The product $\chi_p = -1$ indicates that this system cannot be an insulator, and there is an odd number of band crossings between these two parallel planes [21,22]. The existence of $2n + 1$ ($n \in \mathcal{Z}$) pairs of WPs is realized in FM WSMs with $\mathcal{I}$ symmetry [18,19]. The other is that the planes of $k_3 = 0$ and $k_3 = \pi$ can both be thought as the imaginary Chern insulators, i.e., $\mathcal{C}|_{k_3=0} = \mathcal{C}|_{k_3=\pi} = 1$, which lead to $\chi_p = 1$ [see Fig. 1(b)]. In this case, the system can be either a gapped three-dimensional (3D) Chern insulaor (i.e., 3D quantum anomalous Hall insulator) [30] or a gapless semimetal. When it is a gapless semimetal, band crossings require that there is at least one 2D cut with Chern number $\mathcal{C}|_{k_3=k_i} = 0$ $(0 < k_i < \pi)$ in a reciprocal space; that is, the system can be treated as two subsystems stacking along k_3, sharing the plane of $k_3 = k_i$. Each of the subsystems fits the presence of odd pairs of WPs, i.e., two boundary planes with different Chern numbers (0 and 1). As a result, two band crossings between planes of $k_3 = 0$ and $k_3 = \pi$ are present. In principle, there may also be an even number of eigenvalue switches, i.e., the existence of $2n$ pairs of WPs. In this case, two parallel surfaces with $\mathcal{C} = 0$ may be also present, but there are at least two parallel surfaces with $\mathcal{C} = 1$ [23]. It is worth mentioning that the parity analysis can only allow detecting between $\mathcal{C} = 0$ and $\mathcal{C} = 1$ in FM materials with $\mathcal{I}$ symmetry.

Based on the above discussions, even pairs of WPs in FM WSMs are proposed using the parity argument. Importantly, this inversion eigenvalue argument gives a simple and effective recipe to explore or design the FM WSMs with $\mathcal{I}$ symmetry. Based on this recipe and high-throughput screening of band topology of materials in the inorganic crystal structure database [31], we identify that FM WSMs with even pairs of WPs widely exist in different space groups, such as $C2/m$ (No. 12), $I4/m$ (No. 87), and $R\bar{3}m$ (No. 166). Here, we focus on an experimentally synthesized FM oxide, i.e., hollandite $RbCr_4O_8$. The results of other materials are included in the SM [23]. Remarkably, magnetic measurements show that $RbCr_4O_8$ hosts a FM ground state with $T_c = 295$ K [32,33]. In particular, this exotic topological phase possesses the unconventional twin Weyl fermionic excitations.

To show the band topology of $RbCr_4O_8$, we perform first-principles calculations within the framework of density-functional theory [34,35] as implemented in the Vienna *ab initio* simulation package [36] (see more details in the SM [23]). Because of the correlation effects of $3d$ electrons in Cr atoms, we employ a generalized gradient approximation with Hubbard U parameter (GGA+U) scheme [37] and introduce on site Coulomb repulsion of $U = 3.0$ eV, which is in good agreement with the prior results of the hollandite Cr-O systems [38,39]. The hollandite $RbCr_4O_8$ crystalizes in a monoclinic structure with a space group $C2/m$ (No. 12), as shown in Fig. 2(a). The optimized lattice constants are $a = 14.067$ Å, $b = 3.010$ Å, and $c = 9.985$ Å, which agree well with the experimental values [32]. The bulk Brillouin zone (BZ) and the projected (100) surface BZ are shown in Fig. 2(b).

In the absence of spin orbit coupling (SOC), two spin channels (majority or minority) of $RbCr_4O_8$ do not hybridize with each other, and all crystalline symmetries are preserved for each spin state. $RbCr_4O_8$ hosts an insulating band gap of ~3.7 eV in the minority-spin bands, while the majority-spin bands exhibit the semimetallic features [see Fig. 2(c)]. The complete spin polarization around the Fermi level results in a magnetic moment of ~2.25 μ_B per Cr atom, which shows an excellent agreement with the μ^+SR

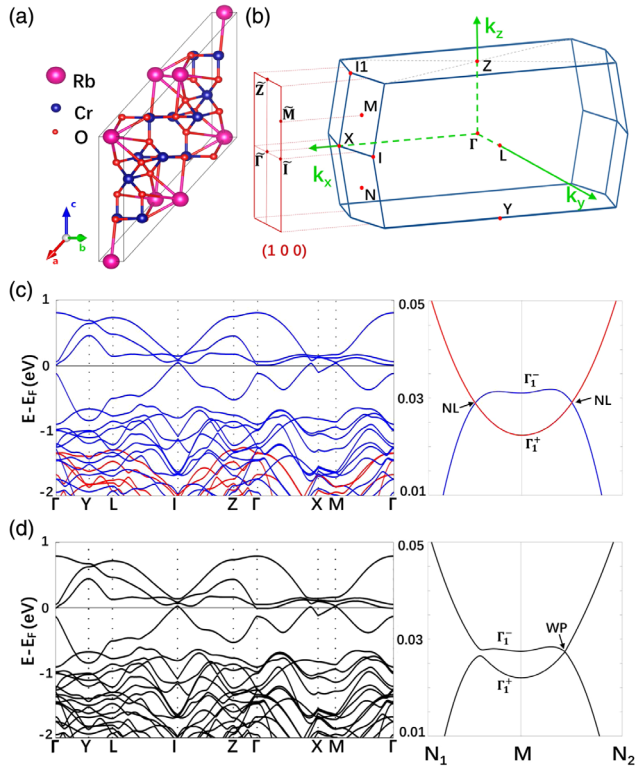

FIG. 2. (a) The hollandite $RbCr_4O_8$ crystalizes in a monoclinic structure with space group $C2/m$ (No. 12). Rb, Cr, and O atoms are represented by pink, blue, and red spheres, respectively. (b) The bulk BZ and (100) surface BZ. (c) Spin-polarized band structure of $RbCr_4O_8$ in the absence of SOC. The right panel of (c) shows the enlargement around the inverted point M. (d) Band structure in the presence of SOC with a magnetization along the $\mathbf{x} = \mathbf{y}$ direction. The right panel of (d) shows that SOC destroys the nodal ring and a WP survives in the M-N_2 direction.

measurement [33]. Two nodal rings are found with the inverted bands centered at the M (0.5, 0.0, 0.5) and Q (0.0, 0.5, 0.5), respectively. As shown in the right panel of Fig. 2(c), we can see that the nodal rings are very closed to the Fermi level, and the maximum energy of crossing points is only ~27 meV above the Fermi level.

Without SOC, the space group $C2/m$ possesses the point group C_{2h}. The symmorphic group elements only contain the inversion $\mathcal{I}$ and mirror M_x. Since the two inverted points M and Q are mirror symmetric in reciprocal space, we mainly focus on the nodal ring around the M point. The two inverted bands can be modeled by the following two-band $k \cdot p$ Hamiltonian,

$$H(\mathbf{q}) = d_0\mathbb{I} + \sum_{i=x,y,z} d_i(\mathbf{q})\sigma_i, \tag{2}$$

where d_0 is the kinetic term, $\mathbb{I}$ is a 2×2 identity matrix, σ_i are Pauli matrices, $d_i(\mathbf{q})$ are real functions of $\mathbf{q}$, and $\mathbf{q} = \mathbf{k} - \mathbf{k}_M$ are three components of the momentum vectors relative to the M point. The little group of the inverted point M is C_i. The two inverted bands at this point have opposite parity, denoted as the irreducible representations Γ_1^+ and Γ_1^-, respectively. The inversion operator can be chosen as $\mathcal{I} = \sigma_z$, which constrains the Hamiltonian as

$$\mathcal{I}H(\mathbf{q})\mathcal{I}^{-1} = H(-\mathbf{q}), \tag{3}$$

which gives

$$d_{0,z}(\mathbf{q}) = d_{0,z}(-\mathbf{q}), \qquad d_{x,y}(\mathbf{q}) = -d_{x,y}(-\mathbf{q}). \tag{4}$$

Besides, in the absence of SOC, $RbCr_4O_8$ can be considered as a spinless ferromagnet, and thus the conservation of spin leads to the spin orientation along an arbitrary direction. Only $\mathcal{T}$ symmetry can translate between a majority-spin state and a minority-spin state, which makes a Hamiltonian invariant as $[H(\mathbf{q}), \mathcal{T}] = 0$ with $\mathcal{T}^2 = 1$. This constraint requires that

$$d_{0,x,z}(\mathbf{q}) = d_{0,x,z}(-\mathbf{q}), \qquad d_y(\mathbf{q}) = -d_y(-\mathbf{q}). \tag{5}$$

Combining Eqs. (4) and (5), we can obtain the symmetry-allowed expressions in the low energy case,

$$\begin{aligned} d_0(\mathbf{q}) &= A_0 + B_0 q_x^2 + C_0 q_y^2 + D_0 q_z^2, \\ d_x(\mathbf{q}) &= 0, \\ d_y(\mathbf{q}) &= B_y q_x + C_y q_y + D_y q_z, \\ d_z(\mathbf{q}) &= A_z + B_z q_x^2 + C_z q_y^2 + D_z q_z^2, \end{aligned} \tag{6}$$

where the $k \cdot p$ parameters can be obtained from the first-principles calculations. Thus, the energy dispersion of the two-band Hamiltonian, Eq. (2), is

$$E(\mathbf{q}) = d_0(\mathbf{q}) \pm \sqrt{d_y(\mathbf{q})^2 + d_z(\mathbf{q})^2}. \tag{7}$$

Based on Eq. (7), the band crossings can be present when $d_y(\mathbf{q}) = 0$ and $d_z(\mathbf{q}) = 0$. This condition has a codimension one, which allows a nodal ring in momentum space. Under the band inversion case, i.e., $A_z < 0$ and B_z, C_z, and $D_z > 0$, $d_z(\mathbf{q}) = 0$, is an equation for a closed ellipsoidal surface surrounding the M point. Meanwhile, $d_y(\mathbf{q}) = 0$ is an equation for a plane with its normal direction (B_y, C_y, D_y) passing the M point. As a result, the crossing points between the closed ellipsoidal surface $d_z(\mathbf{q}) = 0$ and the plane $d_y(\mathbf{q}) = 0$ can form a closed nodal ring. Considering the mirror symmetry M_x, the other nodal ring around the inverted center Q must be present. Expectably, as shown in Figs. 3(a) and 3(b), we can see that two nodal rings are mirror symmetric with respect to the mirror reflection-invariant k_y-k_z plane with $k_x = 0$, forming a mirrored nodal ring pair.

Next, we consider the effects of SOC. The SOC couples the two spin channels and allows them to hybridize. As

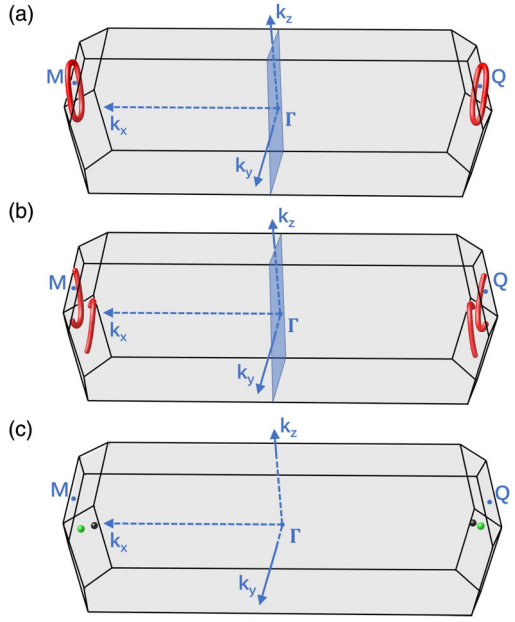

FIG. 3. (a) A pair of nodal rings with respect to the mirror symmetry. The mirror reflection-invariant k_y-k_z plane with $k_x = 0$ is denoted as blue. (b) The mirrored nodal ring pair in the first BZ. (c) In the presence of SOC with a magnetization along the $\mathbf{x} = \mathbf{y}$ direction, the twin Weyl fermionic pairs are present. The WPs with opposite chirality are denoted as the green ($\mathcal{C} = +1$) and black ($\mathcal{C} = -1$) dots, respectively.

shown in Fig. 2(d), we can find that the band structure of $RbCr_4O_8$ with SOC is similar to that without SOC. However, the presence of SOC breaks the spin-rotation symmetry, and then the coupling between spin and electron orbital will induce a magnetization; i.e., the magnetic moments would be favorable to align along a fixed direction. We perform first-principles calculations to determine the magnetization directions, and the results show that the direction of magnetization is isotropic to reside in the ab plane (or xy plane in our case), which is in excellent agreement with the μ^+SR measurement [33].

In the presence of SOC, the symmetry of $RbCr_4O_8$ is reduced to the magnetic point group $C_{2h}(C_i)$. The little group at the inverted points M and Q only contain $\mathcal{I}$ symmetry. The breaking of spin-rotation symmetry can not give an additional constraint on the Hamiltonian Eq. (2), so $d_x(\mathbf{q}) \neq 0$, which can not support a nodal ring in momentum space but can allow the existence of WPs. For example, as shown in the right panel of Fig. 2(d), the nodal point in the N_1-M direction is gapped while the nodal point survives to form a WP in the M-N_2 direction. After a careful check on the band crossing points, we find that each nodal ring evolves into two WPs with opposite chirality [see Fig. 3(c)], forming the exotic twin Weyl fermionic pairs.

In the following, we use the parity analysis to clarify that FM $RbCr_4O_8$ possesses the twin Weyl fermionic pairs (i.e., an even pair of WPs). As shown in Fig. S3 [23], we can easily conclude that there are two parallel planes with Chern number $\mathcal{C} = 1$, such as the $k_1 = 0$ and $k_1 = 0.5$ planes (or $k_2 = 0$ and $k_2 = 0.5$ planes), indicating the presence of an even pair of WPs in $RbCr_4O_8$. To test the topological stability in $RbCr_4O_8$, we respectively apply uniaxial, biaxial, and hydrostatic strains while keeping $\mathcal{I}$ symmetry (see Table S1 and Fig. S2). The results show that the parity eigenvalues at TRIM points are invariant, implying that the twin Weyl fermionic pairs are robustly stable. The parity constraints can also be demonstrated by manipulating the magnetization direction. Since the spin-polarized directions lying in the xy plane are isotropic, we carry out the search of WPs with the magnetization along the $\mathbf{x}$, $\mathbf{y}$ and $\mathbf{x} = \mathbf{y}$ directions, respectively. The twin Weyl fermionic pairs are always present. The orientation of magnetization only shifts the positions of WPs. The momentum coordinates, Chern numbers, and energies related to the Fermi level of WPs along three different magnetic axes are listed in Table I. The Chern numbers are calculated using the Z2Pack package [40], in which the average charge centers obtained from the Wilson-loop method on a sphere around WPs are carried out [41,42].

The local density of states (LDOS) is calculated using the Wannier tight-binding Hamiltonian with the iterative Green's function method [43] as implemented in the WannierTools package [44]. Since the different magnetization directions only shift the positions of WPs and can not essentially affect the topological features, we only pay attention to the surface states with the magnetism oriented in the $\mathbf{x} = \mathbf{y}$ direction. As shown in Fig. 4(a), we show the LDOS projected on the semi-infinite (100) surface. As expected, the nontrivial surface states connect the bulk valence bands and conduction bands, and are terminated at the gapless Weyl cones. Figure 4(b) exhibits the corresponding projected Fermi surface as a function of $E - E_F$. For the energy $E = E_F + 0.027$ eV [see Fig. 4(c)], which corresponds to the location of the WPs, the Fermi arcs connecting the two WPs with opposite chirality are clearly visible, indicating the topological features of twin Weyl fermionic pairs. In addition, the WPs with coordinates $(1.017, 0.233, 0.070)$ Å^{-1} projected on the (100) surface

TABLE I. The momentum coordinates (k_x, k_y, k_z), Chern numbers ($\mathcal{C}$), and energies related to the Fermi level of WPs along different magnetic axes are listed below. The momentum coordinates of other WPs are related to the $\mathcal{I}$ symmetry.

Direction of **M**	Position (Å^{-1})	$E - E_F$ (eV)	$\mathcal{C}$
x	(1.019, 0.160, 0.214)	0.027	−1
	(1.019, −0.160, −0.213)	0.027	−1
y	(1.015, 0.211, 0.086)	0.027	+1
	(1.015, −0.211, −0.086)	0.027	−1
x = **y**	(1.017, 0.233, 0.070)	0.027	+1
	(1.014, −0.194, −0.098)	0.027	−1

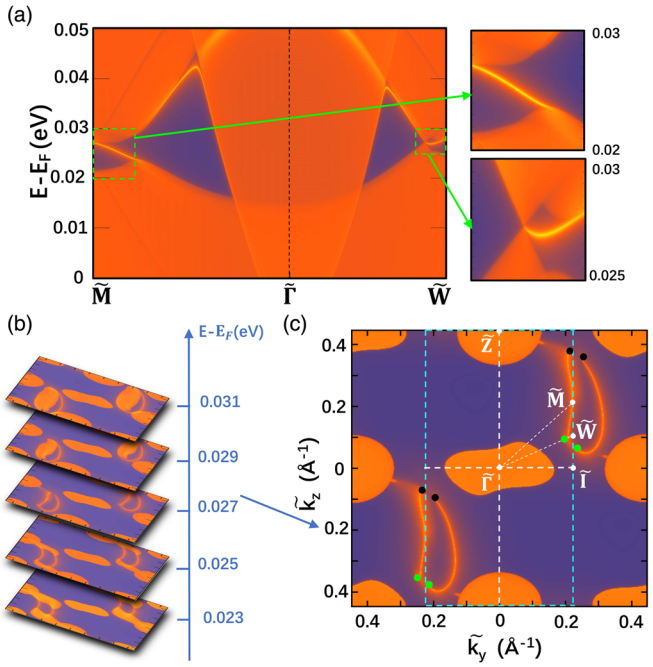

FIG. 4. The surface states and Fermi arcs projected on the semi-infinite (100) surface. (a) LDOS. (b) Projected Fermi surface as a function of $E - E_F$. (c) The Fermi surface at the energy $E = E_F + 0.027$ eV. Fermi arcs connecting the two WPs with opposite chirality are clearly visible. The green and black dots denote the projected WPs with positive and negative chirality, respectively. The first BZ of the (100) surface is marked by blue-dashed box.

will exceed the boundary of the first BZ of this surface. Hence, Fig. 4(c) also shows two extra Fermi arcs in the second BZ of the (100) surface.

In conclusion, we generalize the approach of parity analysis in exploring FM WSMs. The inversion eigenvalue argument suggests that FM WSMs not only possess odd pairs of WPs, but also can possess even pairs of WPs. We identify that FM WSMs with even pairs of WPs widely exist in different space groups. In particular, FM $RbCr_4O_8$ with a high T_c (~295 K), which has already been synthesized in experiments, hosts the twin Weyl fermionic pairs. This exotic nontrivial feature is topologically protected by the parity constraints and is robustly stable against perturbations. We also prove that the twin Weyl fermionic pairs originate from a mirrored nodal ring pair through a combination of effective model and symmetry analysis. Our work can deepen the understanding of FM WSMs with even pairs of WPs and promote the experimental investigations of FM WSMs.

This work is supported by the National Natural Science Foundation of China (NSFC, Grants No. 11674148, No. 11334003, and No. 11847301), the Guangdong Natural Science Funds for Distinguished Young Scholars (No. 2017B030306008), the Fundamental Research Funds for the Central Universities of China (No. 106112017CDJXY300005 and No. cqu2018CDHB1B01), and the Center for Computational Science and Engineering of Southern University of Science and Technology.

B. W. X and Y. J. J equally contributed to this work.

*rcwang@cqu.edu.cn
†xuh@sustc.edu.cn

[1] N. P. Armitage, E. J. Mele, and A. Vishwanath, Rev. Mod. Phys. **90**, 015001 (2018).
[2] Z. Wang, Y. Sun, X.-Q. Chen, C. Franchini, G. Xu, H. Weng, X. Dai, and Z. Fang, Phys. Rev. B **85**, 195320 (2012).
[3] Z. K. Liu, B. Zhou, Y. Zhang, Z. J. Wang, H. M. Weng, D. Prabhakaran, S.-K. Mo, Z. X. Shen, Z. Fang, X. Dai *et al.*, Science **343**, 864 (2014).
[4] X. Wan, A. M. Turner, A. Vishwanath, and S. Y. Savrasov, Phys. Rev. B **83**, 205101 (2011).
[5] A. A. Burkov and L. Balents, Phys. Rev. Lett. **107**, 127205 (2011).
[6] G. Xu, H. Weng, Z. Wang, X. Dai, and Z. Fang, Phys. Rev. Lett. **107**, 186806 (2011).
[7] Y. Xu, F. Zhang, and C. Zhang, Phys. Rev. Lett. **115**, 265304 (2015).
[8] A. A. Soluyanov, D. Gresch, Z. Wang, Q. Wu, and M. Troyer, Nature (London) **527**, 495 (2015).
[9] A. A. Burkov, M. D. Hook, and L. Balents, Phys. Rev. B **84**, 235126 (2011).
[10] Z. Zhu, G. W. Winkler, Q. Wu, J. Li, and A. A. Soluyanov, Phys. Rev. X **6**, 031003 (2016).
[11] S.-S. Wang, Y. Liu, Z.-M. Yu, X.-L. Sheng, and S. A. Yang, Nat. Commun. **8**, 1844 (2017).
[12] B. J. Wieder, Y. Kim, A. M. Rappe, and C. L. Kane, Phys. Rev. Lett. **116**, 186402 (2016).
[13] H. Watanabe, H. C. Po, and A. Vishwanath, Sci. Adv. **4**, eaat8685 (2018).
[14] Z. Song, T. Zhang, and C. Fang, Phys. Rev. X **8**, 031069 (2018).
[15] S.-Y. Xu, I. Belopolski, N. Alidoust, M. Neupane, G. Bian, C. Zhang, R. Sankar, G. Chang, Z. Yuan, C.-C. Lee *et al.*, Science **349**, 613 (2015).
[16] A. Tamai, Q. S. Wu, I. Cucchi, F. Y. Bruno, S. Riccò, T. K. Kim, M. Hoesch, C. Barreteau, E. Giannini, C. Besnard *et al.*, Phys. Rev. X **6**, 031021 (2016).
[17] H. Yang, Y. Sun, Y. Zhang, W.-J. Shi, S. S. P. Parkin, and B. Yan, New J. Phys. **19**, 015008 (2017).
[18] Z. Wang, M. G. Vergniory, S. Kushwaha, M. Hirschberger, E. V. Chulkov, A. Ernst, N. P. Ong, R. J. Cava, and B. A. Bernevig, Phys. Rev. Lett. **117**, 236401 (2016).
[19] Y. J. Jin, R. Wang, Z. J. Chen, J. Z. Zhao, Y. J. Zhao, and H. Xu, Phys. Rev. B **96**, 201102(R) (2017).
[20] R. Wang, Y. J. Jin, J. Z. Zhao, Z. J. Chen, Y. J. Zhao, and H. Xu, Phys. Rev. B **97**, 195157 (2018).
[21] T. L. Hughes, E. Prodan, and B. A. Bernevig, Phys. Rev. B **83**, 245132 (2011).
[22] A. M. Turner, Y. Zhang, R. S. K. Mong, and A. Vishwanath, Phys. Rev. B **85**, 165120 (2012).

[23] See Supplemental Material at http://link.aps.org/supplemental/10.1103/PhysRevLett.122.057205 for the detailed proof of Eq. (1) from parity arguments in a magnetic system with inversion symmetry, parity analysis at the eight TRIM points, the strain effects on the stability of the twin Weyl fermionic pairs in $RbCr_4O_8$, and the brief results of the other candidates with even pairs of WPs. We also give the detailed computational method, which includes Refs. [24–29].
[24] J. P. Perdew, K. Burke, and M. Ernzerhof, Phys. Rev. Lett. **78**, 1396 (1997).
[25] J. P. Perdew, K. Burke, and M. Ernzerhof, Phys. Rev. Lett. **77**, 3865 (1996).
[26] G. Kresse and D. Joubert, Phys. Rev. B **59**, 1758 (1999).
[27] H. J. Monkhorst and J. D. Pack, Phys. Rev. B **13**, 5188 (1976).
[28] A. A. Mostofi, J. R. Yates, D. Vanderbilt, and N. Marzari, Comput. Phys. Commun. **178**, 685 (2008).
[29] N. Marzari, A. A. Mostofi, J. R. Yates, I. Souza, and D. Vanderbilt, Rev. Mod. Phys. **84**, 1419 (2012).
[30] Y. J. Jin, R. Wang, B. W. Xia, B. B. Zheng, and H. Xu, Phys. Rev. B **98**, 081101 (2018).
[31] G. Bergerhoff, R. Hundt, R. Sievers, and I. D. Brown, J. Chem. Inf. Comput. Sci. **23**, 66 (1983).
[32] H. Okada, N. Kinomura, S. Kume, and M. Koizumi, Mater. Res. Bull. **13**, 1047 (1978).
[33] J. Sugiyama, H. Nozaki, M. Månsson, K. Prša, D. Andreica, A. Amato, M. Isobe, and Y. Ueda, Phys. Rev. B **85**, 214407 (2012).
[34] W. Kohn and L. J. Sham, Phys. Rev. **140**, A1133 (1965).
[35] P. Hohenberg and W. Kohn, Phys. Rev. **136**, B864 (1964).
[36] G. Kresse and J. Furthmüller, Phys. Rev. B **54**, 11169 (1996).
[37] A. I. Liechtenstein, V. I. Anisimov, and J. Zaanen, Phys. Rev. B **52**, R5467 (1995).
[38] T. Toriyama, A. Nakao, Y. Yamaki, H. Nakao, Y. Murakami, K. Hasegawa, M. Isobe, Y. Ueda, A. V. Ushakov, D. I. Khomskii *et al.*, Phys. Rev. Lett. **107**, 266402 (2011).
[39] S. Kim, K. Kim, and B. I. Min, Phys. Rev. B **90**, 045124 (2014).
[40] D. Gresch, G. Autès, O. V. Yazyev, M. Troyer, D. Vanderbilt, B. A. Bernevig, and A. A. Soluyanov, Phys. Rev. B **95**, 075146 (2017).
[41] R. Yu, X. L. Qi, A. Bernevig, Z. Fang, and X. Dai, Phys. Rev. B **84**, 075119 (2011).
[42] A. A. Soluyanov and D. Vanderbilt, Phys. Rev. B **83**, 035108 (2011).
[43] M. P. L. Sancho, J. M. L. Sancho, and J. Rubio, J. Phys. F **14**, 1205 (1984).
[44] Q. Wu, S. Zhang, H.-F. Song, M. Troyer, and A. A. Soluyanov, Comput. Phys. Commun. **224**, 405 (2018).